Hindawi Publishing Corporation
Indian Journal of Materials Science
Volume 2016, Article ID 7296847, 7 pages
http://dx.doi.org/10.1155/2016/7296847

Research Article

DFT Study on the Carrier Concentration and Temperature-Dependent Thermoelectric Properties of Antimony Selenide

Aditya Jayaraman, Abhijit Bhat Kademane, and Muralikrishna Molli

Department of Physics, Sri Sathya Sai Institute of Higher Learning, Prasanthi Nilayam 515134, India

Correspondence should be addressed to Muralikrishna Molli; muralikrishnamolli@sssihl.edu.in

Received 14 March 2016; Accepted 8 May 2016

Academic Editor: Federica Bondioli

We present the thermoelectric properties of Antimony Selenide (Sb_2Se_3) obtained using first principles calculations. We investigated the electronic band structure using the FP-LAPW method within the sphere of the density functional theory. Thermoelectric properties were calculated using BoltzTrap code using the constant relaxation time (τ) approximation at three different temperatures 300 K, 600 K, and 800 K. Seebeck coefficient (S) was found to decrease with increasing temperature, electrical conductivity (σ/τ) was almost constant in the entire temperature range, and electronic thermal conductivity (κ/τ) increased with increasing temperature. With increase in temperature S decreased from 1870 μV/K (at 300 K) to 719 μV/K (at 800 K), electronic thermal conductivity increased from 1.56×10^{15} W/m K s (at 300 K) to 3.92×10^{15} W/m K s (at 800 K), and electrical conductivity decreased from $22 \times 10^{19}/\Omega$ m s (at 300 K) to $20 \times 10^{19}/\Omega$ m s (at 800 K). The thermoelectric properties were also calculated for different hole concentrations and the optimum concentration for a good thermoelectric performance over a large range of temperatures (from 300 K to 1000 K) was found for hole concentration around 10^{19} cm^{-3}.

1. Introduction

Thermoelectric (TE) materials are a wonderful class of materials that enable us to have direct conversion from heat to electricity and vice versa. The efficiency of a thermoelectric material is characterized by a dimensionless parameter called the figure of merit:

$$zT = \frac{S^2 \sigma T}{\kappa_{\text{el}} + \kappa_l}, \tag{1}$$

where S is the Seebeck coefficient, T is temperature, σ is electrical conductivity, and κ_{el} and κ_l are the electron and phonon contributions to total thermal conductivity.

To have the maximum figure of merit, one needs a material with large Seebeck coefficient, large electrical conductivity, and low thermal conductivity.

The A_2B_3 (A = Sb and Bi; B = S, Se, and Te) series consists of layered chalcogenide semiconductors that have attracted considerable interest, mainly due to their exceptional thermoelectric properties. More recently, three members of this series, namely, the Bi_2Te_3, Sb_2Te_3, and Bi_2Se_3 compounds, were shown to exhibit topological insulating properties [1, 2]. This discovery has revitalized the scientific interest in these materials. At ambient conditions, the A_2B_3 (A = Sb and Bi; B = S, Se, and Te) family is divided into two structural classes: the heavier Bi_2Se_3, Bi_2Te_3, and Sb_2Te_3 compounds adopt a rhombohedral structure (space group R-3m), which is composed of layers of AB_6 octahedra stacked perpendicular to the long c-axis; the lighter Bi_2S_3, Sb_2S_3, and Sb_2Se_3 materials on the other hand, crystallize in an orthorhombic phase (space group Pnma, U_2S_3-type), made up of AB_7 and AB_{7+1} polyhedra.

Sb_2Se_3 is a promising TE material with a high Seebeck coefficient ~1800 μV/K, but its figure of merit is limited by its low electrical conductivity which is ~10^{-6} to 10^{-2} Ω^{-1} m^{-1} for bulk Sb_2Se_3 at 300 K [3–5]. In order to improve its TE performance, various nanostructures of the material have

Table 1: Fractional coordinates of atoms in Sb_2Se_3 unit cell.

Atom	WYCOFF positions	X	Y	Z
Sb(1)	4c	0.5304	0.25	0.1721
Sb(2)	4c	0.6475	0.75	0.4604
Se(1)	4c	0.6289	0.75	0.0553
Se(2)	4c	0.7141	0.25	0.3051
Se(3)	4c	0.4464	0.75	0.3713

been investigated. Hanifehpour et al. [6] reported electrical conductivity of pure Sb_2Se_3 nanorods (5 μm length and 25–120 nm thickness) to be 5 Ω^{-1} m^{-1} at room temperature. Wang et al. [7] presented electrical conductivity (0.6 Ω^{-1} m^{-1} at 300 K) and Seebeck coefficient (–1260 μV/K) of Sb_2Se_3 films (2-3 μm thick) consisting of Sb_2Se_3 nanowires. Mehta et al. [8] investigated individual 1D sulfurized Sb_2Se_3 nanostructure (dia > 30 nm) prepared by microwave assisted solvothermal method with Seebeck coefficient ~750 μV/K and electrical conductivity of 10–10^4 Ω^{-1} m^{-1}. But so far there are no studies on this material in terms of the transport properties calculations theoretically. So we went on to investigate the electronic band structure and further calculate the thermoelectric transport properties.

At ambient conditions, Sb_2Se_3 adopts an orthorhombic structure (U_2S_3-type, space group: 62.Pnma). There are two nonequivalent Sb cation sites in this phase. One of the Sb cations is coordinated by seven Se anions and the coordination around the second Sb site can be described as (7 + 1) with respect to the Se ions [9].

The fractional coordinates of atoms in a unit cell of Sb_2Se_3 [10] are given in Table 1.

2. Computational Details

Sb_2Se_3 has an orthorhombic structure belonging to 62.Pnma space group. Experimental lattice parameters were used for computation [10, 11]. The band structure of Sb_2Se_3 was calculated under the purview of density functional theory using the WIEN2k [12] package which uses FP-LAPW (Full Potential Linear Augmented Plane Wave) method with local orbitals. In this method, the wave functions are expanded in spherical harmonics inside nonoverlapping atomic spheres of radius RMT and in plane waves in the interstitial region. The PBE (Perdew, Burke, and Ernzerhof) and mBJ (modified Becke-Johnson) exchange correlation potentials were used for calculations. The RK_{max} (the product of RMT_{min} and K_{max}) value was chosen to be 8. The maximum value of l (l_{max}) for the expansion of spherical harmonics in the atomic spheres is taken as 10. A k mesh of 3000 k points was used in the first Brillouin zone.

The transport properties such as Seebeck coefficient, electrical conductivity, and electronic thermal conductivity were calculated using the BoltzTraP code [13] that solves the semiclassical Boltzmann transport equation under the constant relaxation time (τ) approximation. A dense k mesh of 50,000 k points in the first Brillouin zone was used for transport properties calculation. Lpfac (lattice points factor) value of 5 was used in these calculations. In the constant relaxation time approximation S is independent of τ while σ, κ, and power factor $S^2\sigma$ can only be obtained in units of τ. To obtain their actual values, one may either use experimental values of τ if available or use available models for energy and temperature-dependent relaxation time in simpler systems like PbTe [14, 15]. Since there is no experimental data available on the relaxation time in this material, we only give the electrical conductivity, electronic thermal conductivity, and thermoelectric power factor scaled in terms of τ.

3. Results and Discussion

3.1. Band Structure and Density of States. The band structure of Sb_2Se_3 was calculated along the high symmetry points of the Brillouin zone. The band structures were calculated using PBE and mBJ exchange correlation potential (Figures 1(a) and 1(b)). The band gap of Sb_2Se_3 according to the PBE was found to be ~0.9 eV. The experimental indirect band gap observed was around 1.2 eV [16] which is obtained from allowed indirect Tauc plot fitting of optical absorption spectrum [17]. The Tauc equation used for determining the indirect band gap from optical absorption spectrum is given by

$$(\alpha h\upsilon)^{1/2} = \text{const.}\left(h\upsilon - E_g\right), \tag{2}$$

where $h\upsilon$ is the photon energy and E_g is the indirect energy band gap.

So using the PBE exchange correlation potential, the band gap is underestimated. From the analysis of band structure using mBJ potential, we observe that it is an indirect band gap semiconductor with a band gap of 1.21 eV which is closer to the experimental value [18].

The total density of states was also calculated and is shown in Figure 2. From the total density of states plot, it is evident that the valence and conduction band are equally dense near the band edge. Also a band gap of 1.20 eV can be observed between the band edges.

3.2. Thermoelectric Properties

3.2.1. Transport Properties as a Function of Chemical Potential. The thermoelectric properties were calculated using the BoltzTraP code in the constant relaxation time approximation. The calculated properties were plotted as a function of chemical potential at 300 K, 600 K, and 800 K.

Before presenting the calculated results we discuss briefly what is meant by chemical potential and what factors affect its value.

The chemical potential determines the center of the Fermi-Dirac distribution function. In case of electrons, the probability of occupancy of a quantum state with energy E is given by the Fermi-Dirac distribution function $f(E) = 1/(1+\exp((E-\mu)/kT))$, where μ is the chemical potential. The total number of electrons per unit volume in a crystal is given by $n = \int_0^\infty f(E,T,\mu)D(E)dE$, where $D(E)$ is the density of states and $f(E,T,\mu)$ is the Fermi-Dirac distribution function.

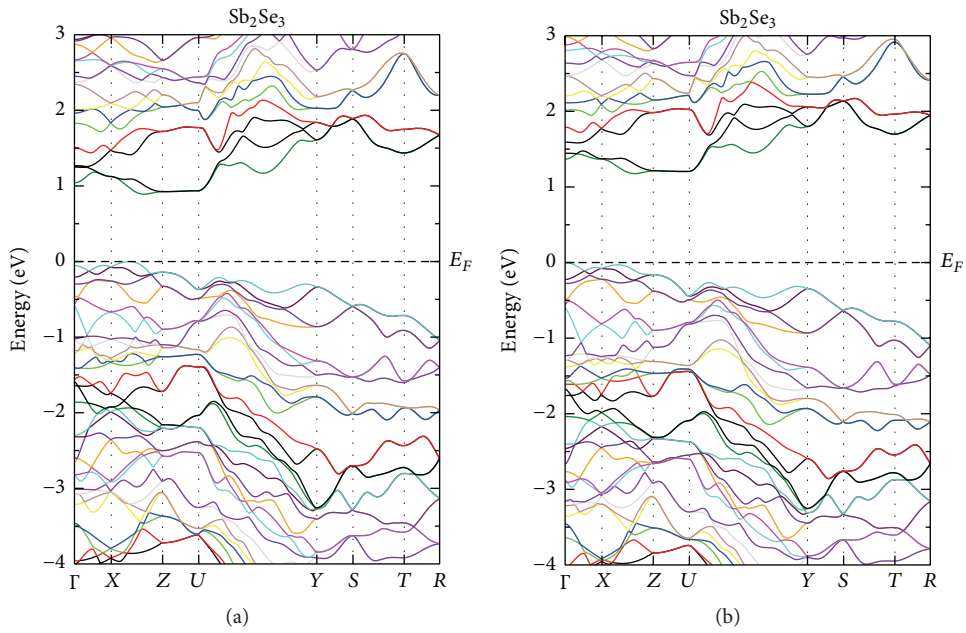

FIGURE 1: Band structure of Sb_2Se_3 using (a) PBE potential and (b) mBJ potential.

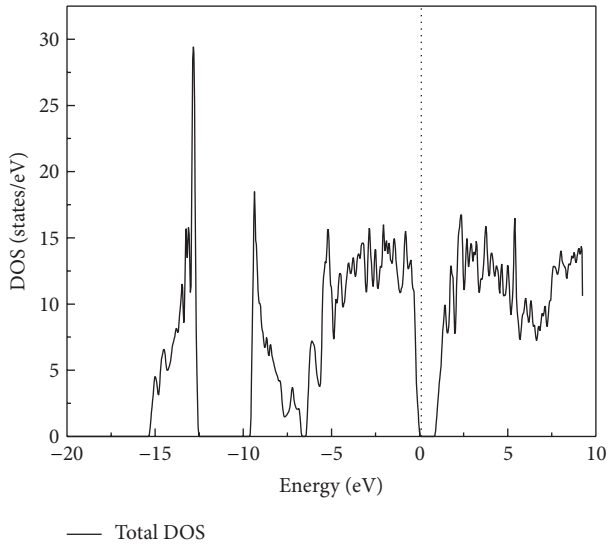

FIGURE 2: Total density of states of Sb_2Se_3 (calculated using mBJ exchange correlation potential).

This equation determines the chemical potential as a function of temperature for a given carrier concentration n.

When $((E - \mu)/kT) \gg 1$, which is the classical limit, Boltzmann distribution is used as an approximation to the Fermi-Dirac distribution and we get $n = N_c \exp(-(E_c - \mu)/kT)$, where $N_c = 2(2\pi m^* kT/h^2)^{3/2}$. This equation is often used to determine the chemical potential level in doped semiconductors [19].

The position of chemical potential (μ) plays an important role with regard to the transport properties. Position of μ in the band structure determines which electrons in the valence or conduction band take part in the electronic transport and thus influences both the conductivity and the Seebeck coefficient. Doping or substitution is used to manipulate the chemical potential by varying the number of valence electrons in compounds and alloys. By definition, $\mu = 0$ corresponds to the top of the valence band in semiconductors [20]. Chemical potential is determined by the temperature and by the total number of carriers. The behaviour of the chemical potential with varying temperature and doping is interesting with regard to thermoelectric properties. Figure 9 shows the calculated variation of chemical potential with respect to temperature in the case of Sb_2Se_3. It has a slight variation with respect to temperature.

From the Seebeck plot (Figure 3) it is clear that at $\mu = 0$, the value of Seebeck coefficient is 222 μV/K (at $T = 300$ K). Hence, it is a p-type semiconductor (since $S > 0$ at $\mu = 0$). Also, maximum value of S (1870 μV/K) at 300 K is close to the value of 1800 μV/K reported experimentally [8]. Seebeck coefficient (S) was found to decrease with increasing temperature: with increase in temperature S decreased from 1870 μV/K (at 300 K) to 719 μV/K (at 800 K).

Electrical conductivity (σ/τ, Figure 4) is almost independent of temperature. The maximum value of electrical conductivity of 2.25×10^{20} Ω^{-1} m^{-1} s^{-1} occurs at $\mu = 0.19$ Ry (1 Ry = 13.6 eV). Electrical conductivity decreased from 22×10^{19}/Ω m s (at 300 K) to 20×10^{19}/Ω m s (at 800 K).

The electronic thermal conductivity (κ/τ, Figure 5) is found to increase with temperature. Electronic thermal conductivity increased from 1.56×10^{15} W/m K s (at 300 K) to 3.92×10^{15} W/m K s (at 800 K).

From the plot of thermoelectric power factor ($(S^2\sigma/\tau)$, Figure 6), it is evident that it is highest for n-type Sb_2Se_3

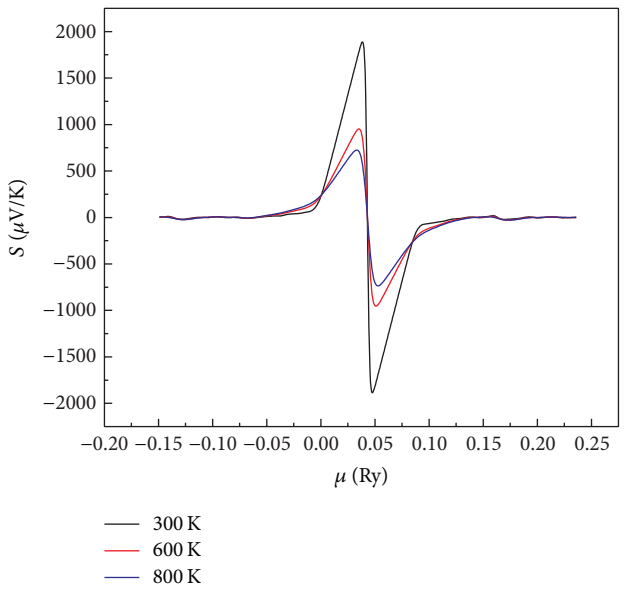

Figure 3: Variation of Seebeck coefficient with respect to chemical potential.

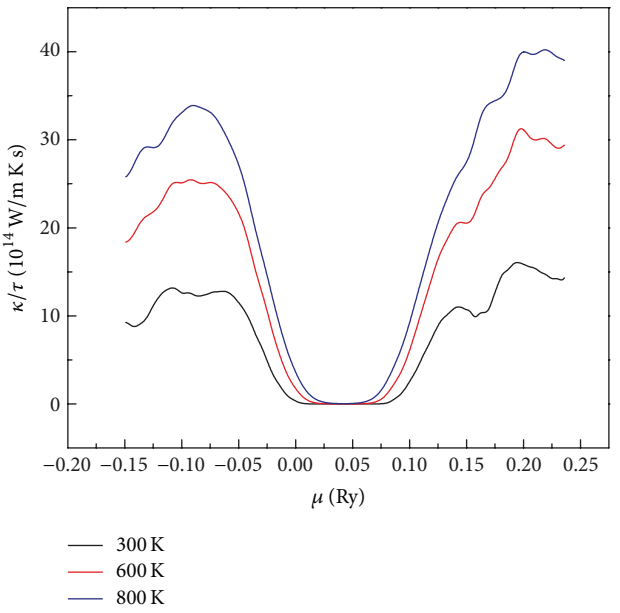

Figure 5: Variation of electronic thermal conductivity (κ/τ) with respect to chemical potential.

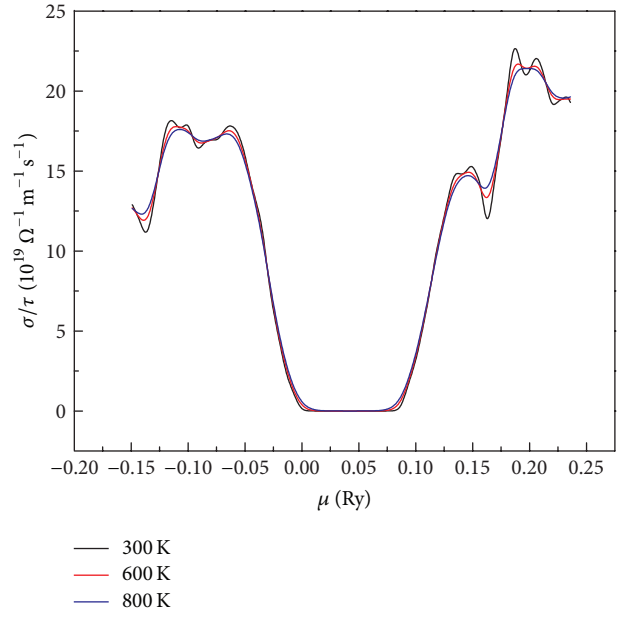

Figure 4: Variation of electrical conductivity (σ/τ) with respect to chemical potential.

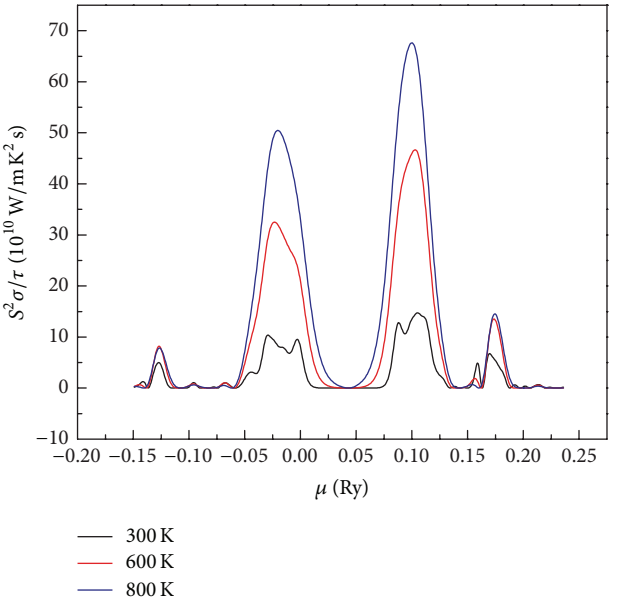

Figure 6: Variation of thermoelectric power factor ($S^2\sigma/\tau$) with respect to chemical potential.

($\sim 67 \times 10^{10}$ W m^{-1} K^{-2} s^{-1}) at $\mu = 0.12$ Ry at 800 K. For p-type Sb_2Se_3, the maximum value is exhibited at $\mu = -0.025$ Ry at 800 K.

3.2.2. Variation of Transport Properties with Temperature at Various Hole Concentrations. The various thermoelectric (TE) properties were calculated with respect to temperature by fixing the concentration of the amount of hole doping. The TE properties were calculated for doping concentrations of 10^{16} cm^{-3}, 10^{17} cm^{-3}, 10^{18} cm^{-3}, and 10^{19} cm^{-3}.

From Figure 7(b), we observe that till a certain temperature, the conductivity is independent of temperature (e.g., for $p = 10^{16}$ cm^{-3}, till 600 K the conductivity is constant). But as the temperature is increased further, bipolar transport sets up, leading to exponential increase in the conductivity [21].

The same is the case for the electronic thermal conductivity. As the concentration is increased, the recombination rate increases. Thus, the bipolar transport is set up at a considerably higher temperature. As the concentration is increased from 10^{16} cm^{-3} to 10^{18} cm^{-3}, the temperature at

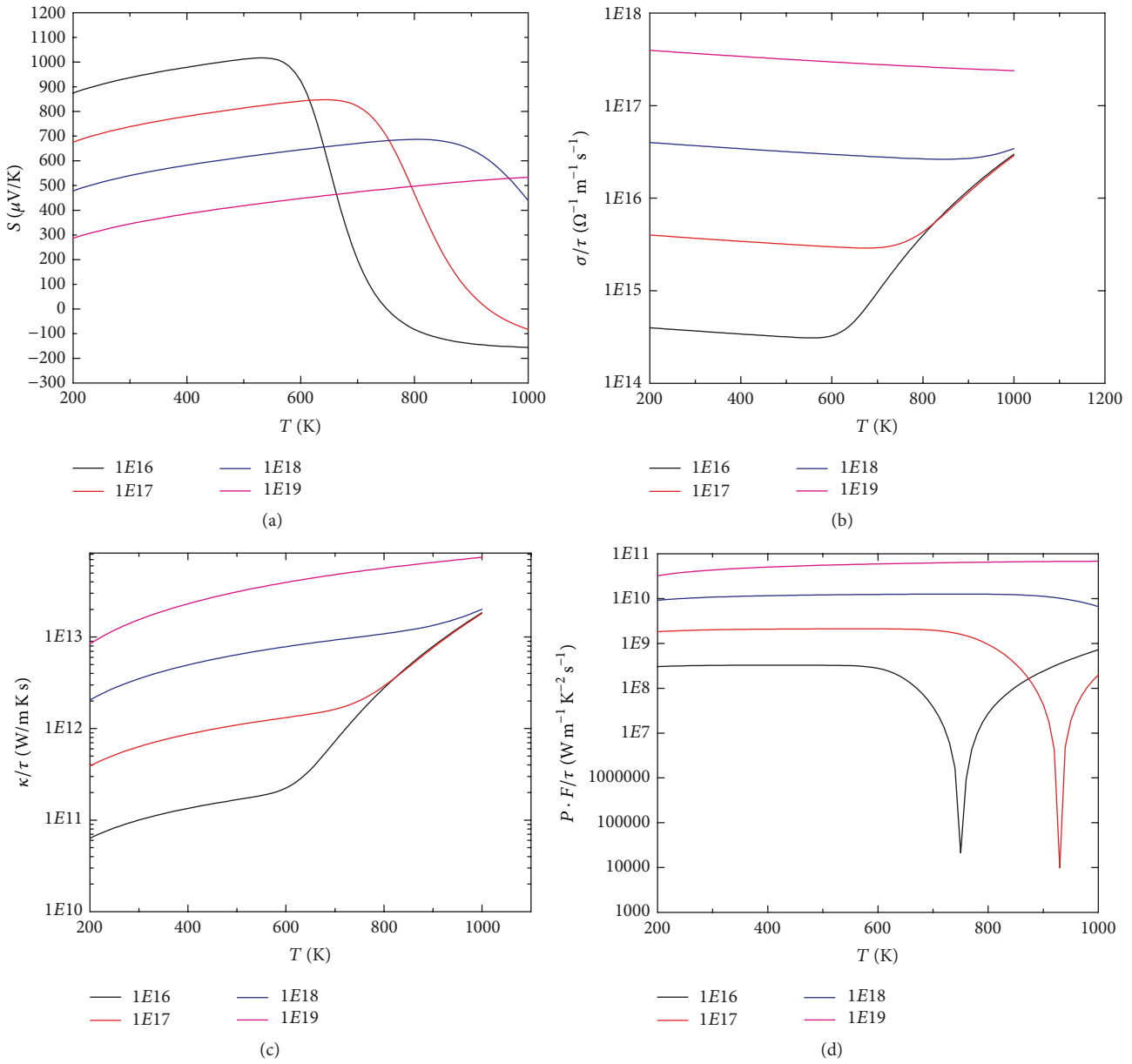

FIGURE 7: (a) Seebeck coefficient, (b) electrical conductivity, (c) electronic thermal conductivity, and (d) power factor with respect to temperature at various hole doping concentrations.

which the bipolar transport is set up increases from ~600 K to ~850 K.

The Seebeck coefficient (Figure 7(a)) is almost constant till a particular temperature. But as the bipolar transport is set up, the Seebeck coefficient decreases. This is because of the opposing nature of the currents setup by electrons and holes due to thermal gradient.

Also, we can observe that at high temperatures, the Seebeck coefficient is negative. This is attributed to the fact that the thermally excited electrons start to dominate transport and the semiconductor changes from *p*-type to *n*-type.

From the power factor graph (Figure 7(d)), we see a dip at 740 K for a concentration of 10^{16} cm^{-3}. This dip is because of change in the sign of Seebeck coefficient at this temperature. Beyond this dip, the value of Seebeck coefficient is negative.

At lower temperatures, the Seebeck coefficient monotonically decreases with increasing hole concentration (Figure 8). At high temperatures, however, there is an optimum concentration of holes at which the Seebeck coefficient is highest. It corresponds to ~5×10^{17} cm^{-3} holes (at 800 K).

4. Conclusion

The study of Sb_2Se_3 using the density functional theory proved insightful. It has been observed that Sb_2Se_3 shows optimal thermoelectric performance at high temperatures (~800 K) for a doping concentration of ~10^{19} cm^{-3} holes.

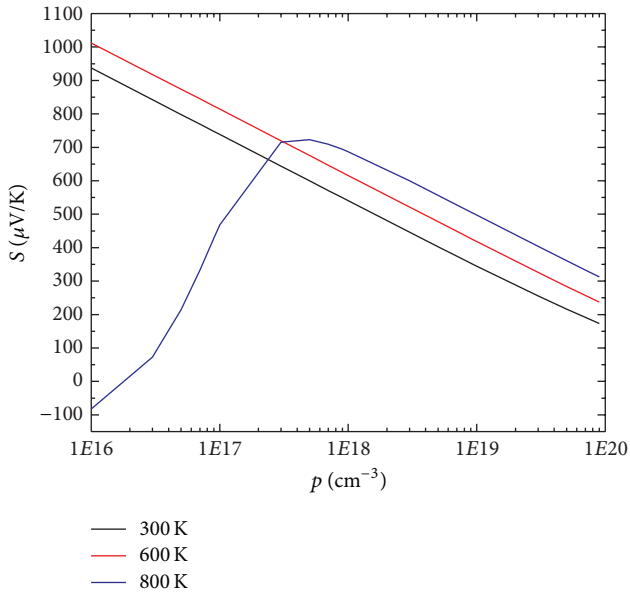

Figure 8: Plot of Seebeck coefficient versus hole concentration at different temperatures.

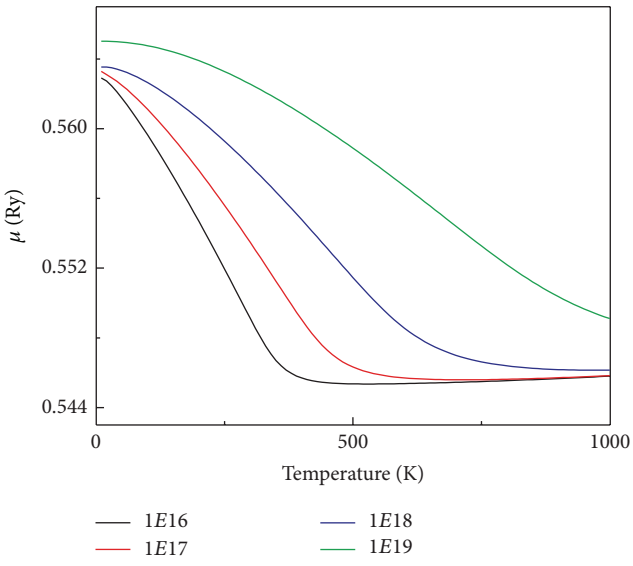

Figure 9: Variation of chemical potential with respect to temperature for different hole doping concentrations.

Competing Interests

The authors declare that there are no competing interests regarding the publication of this paper.

Acknowledgments

The authors express their sincere gratitude to Bhagawan Sri Sathya Sai Baba, the Founder Chancellor of SSSIHL, for his constant support and lab facilities. The authors acknowledge the financial support from DST-FIST (sanction no. SR/FST/PSI-172/2012). The author Muralikrishna Molli expresses special thanks to Council of Scientific and Industrial Research (CSIR) (CSIR Award no. 09/982(0001)/2009-EMR-I), Government of India, for the award of Research Fellowship.

References

[1] Y. L. Chen, J. G. Analytis, J.-H. Chu et al., "Experimental realization of a three-dimensional topological insulator, Bi_2Te_3," *Science*, vol. 325, no. 5937, pp. 178–181, 2009.

[2] H. Zhang, C.-X. Liu, X.-L. Qi, X. Dai, Z. Fang, and S.-C. Zhang, "Topological insulators in Bi_2Se_3, Bi_2Te_3 and Sb_2Te_3 with a single Dirac cone on the surface," *Nature Physics*, vol. 5, no. 6, pp. 438–442, 2009.

[3] L. G. Gribnyak and T. B. Ivanova, "Electrical properties of single crystal antimony selenide," *Inorganic Materials*, vol. 23, pp. 478–482, 1987.

[4] B. R. Chakraborty, B. Ray, R. Bhattacharya, and A. K. Dutta, "Magnetic and electric properties of antimony selenide (Sb_2Se_3) crystals," *Journal of Physics and Chemistry of Solids*, vol. 41, no. 8, pp. 913–917, 1980.

[5] X. W. Zheng, Y. Xie, L. Y. Zhu et al., "Growth of Sb_2E_3 (E = S, Se) polygonal tubular crystals via a novel solvent-relief-self-seeding process," *Inorganic Chemistry*, vol. 41, no. 3, pp. 455–461, 2002.

[6] Y. Hanifehpour, S. W. Joo, and B.-K. Min, "Lu^{3+}/Yb^{3+} and Lu^{3+}/Er^{3+} co-doped antimony selenide nanomaterials: synthesis, characterization, and electrical, thermoelectrical, and optical properties," *Nanoscale Research Letters*, vol. 8, no. 1, article 141, 2013.

[7] X. Wang, K. F. Cai, F. Shang, and S. Chen, "Preparation and electrical transport properties of nanostructured Sb_2Se_3 films fabricated by combining spin-coating and gas-induced reduction," *Journal of Nanoparticle Research*, vol. 15, article 1541, 2013.

[8] R. J. Mehta, C. Karthik, W. Jiang et al., "High electrical conductivity antimony selenide nanocrystals and assemblies," *Nano Letters*, vol. 10, no. 11, pp. 4417–4422, 2010.

[9] I. Efthimiopoulos, J. Zhang, M. Kucway, C. Park, R. C. Ewing, and Y. Wang, "Sb_2Se_3 under pressure," *Scientific Reports*, vol. 3, article 2665, 2013.

[10] R. Caracas and X. Gonze, "First-principles study of the electronic properties of A_2B_3 minerals, with A=Bi,Sb and B=S,Se," *Physics and Chemistry of Minerals*, vol. 32, no. 4, pp. 295–300, 2005.

[11] L.-D. Zhao, S.-H. Lo, Y. Zhang et al., "Ultralow thermal conductivity and high thermoelectric figure of merit in SnSe crystals," *Nature*, vol. 508, no. 7496, pp. 373–377, 2014.

[12] P. Blaha, K. Schwarz, G. Madsen, D. Kvasnicka, and J. Luitz, WIEN2k, An Augmented Plane Wave + Local Orbitals Program for Calculating Crystal Properties (Karlheinz Schwarz, Techn. Universität Wien, Austria), 2001.

[13] G. K. H. Madsen and D. J. Singh, "BoltzTraP. A code for calculating band-structure dependent quantities," *Computer Physics Communications*, vol. 175, no. 1, pp. 67–71, 2006.

[14] Y. O. Ciftci and S. D. Mahanti, "Electronic structure and thermoelectric properties of half-Heusler compounds with eight electron valence count—KScX (X = C and Ge)," *Journal of Applied Physics*, vol. 119, Article ID 145703, 2016.

[15] S. Ahmad and S. D. Mahanti, "Energy and temperature dependence of relaxation time and Wiedemann-Franz law on PbTe," *Physical Review B*, vol. 81, no. 16, Article ID 165203, 2010.

[16] L. R. Gilbert, B. Van Pelt, and C. Wood, "The thermal activation energy of crystalline Sb_2Se_3," *Journal of Physics and Chemistry of Solids*, vol. 35, no. 12, pp. 1629–1632, 1974.

[17] J. I. Pankove, *Optical Processes in Semiconductors*, Dover, New York, NY, USA, 1971.

[18] R. Vadapoo, S. Krishnan, H. Yilmaz, and C. Marin, "Electronic structure of antimony selenide (Sb_2Se_3) from GW calculations," *Physica Status Solidi B*, vol. 248, no. 3, pp. 700–705, 2011.

[19] G. Chen, *Nanoscale Energy Transport and Conversion*, Oxford University Press, 2005.

[20] G. H. Fecher, E. Rausch, B. Balke, A. Weidenkaff, and C. Felser, "Half-Heusler materials as model systems for phase-separated thermoelectrics," *Physica Status Solidi (A)*, vol. 213, no. 3, pp. 716–731, 2016.

[21] G. Shi and E. Kioupakis, "Quasiparticle band structures and thermoelectric transport properties of p-type SnSe," *Journal of Applied Physics*, vol. 117, no. 6, Article ID 065103, 2015.